Poly(Sarcosine)-Based Nano-Objects with Multi-Protease Resistance by Aqueous Photoinitiated Polymerization-Induced Self-Assembly (Photo-PISA)

Varlas, Spyridon; Georgiou, Panagiotis G; Bilalis, Panayiotis; Jones, Joseph R; Hadjichristidis, Nikos; O'Reilly, Rachel K

DOI:
10.1021/acs.biomac.8b01326

Article

Poly(Sarcosine)-Based Nano-Objects with Multi-Protease Resistance by Aqueous Photoinitiated Polymerization-Induced Self-Assembly (Photo-PISA)

Spyridon Varlas, Panagiotis G. Georgiou, Panayiotis Bilalis, Joseph R. Jones, Nikos Hadjichristidis, and Rachel K. O'Reilly

Biomacromolecules, **Just Accepted Manuscript** • DOI: 10.1021/acs.biomac.8b01326 • Publication Date (Web): 23 Oct 2018

Poly(Sarcosine)-Based Nano-Objects with Multi-Protease Resistance by Aqueous Photoinitiated Polymerization-Induced Self-Assembly (Photo-PISA)

Spyridon Varlas,[a] Panagiotis G. Georgiou,[a,b] Panayiotis Bilalis,[c] Joseph R. Jones,[a] Nikos Hadjichristidis,[c] and Rachel K. O'Reilly[a]**

[a] School of Chemistry, University of Birmingham, B15 2TT, Birmingham, UK

[b] Department of Chemistry, University of Warwick, Gibbet Hill Road, CV4 7AL, Coventry, UK

[c] Physical Sciences and Engineering Division, KAUST Catalysis Center, Polymer Synthesis Laboratory, King Abdullah University of Science and Technology (KAUST), 23955, Thuwal, Saudi Arabia

**Corresponding Authors*: nikolaos.hadjichristidis@kaust.edu.sa (N.H.) and r.oreilly@bham.ac.uk (R.K.O.R.)

KEYWORDS

polymerization-induced self-assembly (PISA), ring-opening polymerization (ROP), reversible addition-fragmentation chain-transfer (RAFT) polymerization, photoinitiated polymerization, poly(sarcosine), protease resistance.

ABSTRACT

Poly(sarcosine) (PSar) is a non-ionic hydrophilic poly(peptoid) with numerous biologically relevant properties, making it an appealing candidate for the development of amphiphilic block copolymer nanostructures. In this work, the fabrication of poly(sarcosine)-based diblock copolymer nano-objects with various morphologies *via* aqueous reversible addition-fragmentation chain-transfer (RAFT)-mediated photoinitiated polymerization-induced self-assembly (photo-PISA) is reported. Poly(sarcosine) was first synthesized *via* ring-opening polymerization (ROP) of sarcosine *N*-carboxyanhydride, using high-vacuum techniques. A small molecule chain transfer agent (CTA) was then coupled to the active ω-amino chain end of the telechelic polymer for the synthesis of a poly(sarcosine)-based macro-CTA. Controlled chain-extensions of a commercially available water-miscible methacrylate monomer (2-hydroxypropyl methacrylate) were achieved *via* photo-PISA under mild reaction conditions, using PSar macro-CTA. Upon varying the degree of polymerization and concentration of the core-forming monomer, morphologies evolving from spherical micelles to worm-like micelles and vesicles were accessed, as determined by dynamic light scattering and transmission electron microscopy, resulting in the construction of a detailed phase diagram. The resistance of both colloidally stable empty vesicles and enzyme-loaded nanoreactors against degradation by a series of proteases was finally assessed. Overall, our findings underline the potential of poly(sarcosine) as an alternative corona-forming polymer to poly(ethylene glycol)-based analogues of PISA assemblies for use in various pharmaceutical and biomedical applications.

INTRODUCTION

In modern polymer and materials science, poly(ethylene glycol) (PEG) and ethylene glycol-based polymers mainly from meth(acrylate) monomers are considered the gold standard for the design of nanostructures and materials with "stealth-like" properties.[1-3] PEG is widely utilized in various biotechnological applications such as drug/protein delivery and targeted diagnostics,[4, 5] surface coatings,[6] household and personal care products,[7, 8] and cell cryopreservation.[9] This is mainly attributed to the high flexibility and hydrophilicity, low cellular toxicity and biocompatible character of PEG that make it an efficient material for such applications.[10] However, PEG is known to be a non-bio-based and non-biodegradable polymer with limited functionality, while studies have also shown oxidative activity of PEG in physiological cellular environments, immune response of patients and accelerated blood clearance phenomena caused by anti-PEG antibodies.[11-14] Consequently, in recent years there is a growing demand for finding alternatives to overcome these limitations of PEG.[15]

A broad variety of hydrophilic polymers including poly(glycerols),[16] poly(oxazolines),[17] poly(peptides)[18] and poly(peptoids)[19] with comparable physicochemical properties to PEG have been currently explored and proposed as promising alternatives. Among them, poly(peptoids), an important family of biomaterials, only recently have attracted the attention of scientific community.[19, 20] Poly(sarcosine) (PSar), also referred as poly(*N*-methylated glycine), is the simplest member of the poly(peptoid) family that displays PEG-like properties and is based on an achiral endogenous but non-proteinogenic amino acid, sarcosine, mainly found in muscle tissues.[21, 22] N-Substitution of amino acid residues in poly(peptoids) is a common synthetic procedure to promote the random coil conformation over other secondary structures (e.g. α-helices

and β-sheets) and to confer substantial flexibility to the polymer chains thus enhancing the resistance of the derived materials toward enzymatic degradation.[20, 23] PSar is a non-ionic, hydrophilic, highly biocompatible and potentially biodegradable polymer that exhibits low cellular toxicity, limited interactions with blood components and "stealth-like" non-immunogenic character.[23, 24] In addition to aqueous solubility, PSar is also highly soluble in common polar organic solvents. Moreover, PSar can be synthesized *via* living ring-opening polymerization (ROP) of the corresponding *N*-carboxyanhydride (NCA) to produce well-defined telechelic homo- and copolymers with low dispersities.[25, 26] Further post-polymerization modification of the living amino-terminal chain end allows for the insertion of various functionalities and the combination of PSar with other synthetic polymers. Overall, the unique features of PSar suggest that it can be effectively utilized as a PEG-alternative corona-forming block imparting higher colloidal stability (i.e. prevention of protein-induced aggregation), minimal systemic toxicity and longer circulation times *in vivo* to amphiphilic block copolymer assemblies.[23]

Over the last years, studies on the synthesis and self-assembly behavior of PSar-based block copolymers for the development of nanostructures of biotechnological interest have been presented, although they involve the use of conventional self-assembly procedures in dilute aqueous solutions.[13, 23, 27-32] Recently, polymerization-induced self-assembly (PISA) has been established as an efficient methodology for facile one-pot fabrication of polymeric nano-objects with predictable morphologies at high solids concentrations (10-50% w/w).[33-36] Existing limitations of traditional self-assembly strategies (i.e. direct dissolution, thin-film hydration, and solvent-switch) such as low polymer concentrations (≤1% w/w) and laborious post-polymerization processing steps for targeting certain morphologies are proven to be overcome by PISA. Only selected monomers have the ability to undergo PISA

since a solubility transition of the gradually growing core-forming block from solvent-soluble to solvent-immiscible is required.[34] In principle, PISA can be achieved by using any known polymerization technique, although the vast majority of PISA studies to date involve implementation of reversible-deactivation radical polymerization (RDRP) techniques, including atom transfer radical polymerization (ATRP),[37, 38] nitroxide-mediated polymerization (NMP),[39, 40] and reversible addition-fragmentation chain-transfer (RAFT) polymerization,[41-44] under either dispersion or emulsion polymerization conditions, owing to their versatility and broad applicability. Ring-opening metathesis polymerization (ROMP) has been also introduced lately as a non-radical approach for PISA in both aqueous and organic media.[45-47]

In particular, there has been rapidly growing research interest in aqueous RAFT-mediated photoinitiated PISA (photo-PISA) *via* either the well-described "photoiniferter" mechanism of chain transfer agents (CTAs) or by using special photoinitiators and photoredox catalysts under ultraviolet or visible-light irradiation.[42, 48-54] This is mainly attributed to the ambient temperatures and mild reaction conditions of photo-PISA that are not harmful to sensitive biomolecules (i.e. drugs, enzymes, membrane proteins) enabling their direct encapsulation into well-defined polymeric vesicles for the one-pot development of cargo-loaded delivery vehicles and nanoreactors of further bio-related interest.[55-59]

Herein, the preparation of diblock copolymer nano-objects with different morphologies bearing a PSar hydrophilic corona *via* a combination of NCA ROP and RAFT-mediated photo-PISA is reported. First, sarcosine NCA (Sar NCA) was synthesized from the corresponding *N*-Boc-protected amino acid. Living ROP of Sar NCA using high-vacuum techniques and an amino initiator yielded an ω-telechelic PSar homopolymer with monomodal molecular weight

distribution and low dispersity ($Đ_M$). Due to the absence of side chain functional groups found in poly(peptides), quantitative coupling between an acid-functionalized small molecule CTA and the sterically accessible N-terminus of PSar was achieved, resulting in the formation of a water-soluble PSar macromolecular CTA (macro-CTA). As a next step, PSar macro-CTA was used to carry out aqueous photo-PISA reactions of 2-hydroxypropyl methacrylate (HPMA) under dispersion polymerization conditions by varying PHPMA degrees of polymerization and total solids concentration (Scheme 1). The obtained PSar-*b*-PHPMA diblock copolymer assemblies were characterized by dynamic light scattering (DLS), zeta-potential analysis and transmission electron microscopy (TEM) imaging, resulting in the construction of a morphologies diagram. To further explore the robust nature and PEG-like characteristics of PSar-based nano-objects, the colloidal stability of PSar-*b*-PHPMA unilamellar vesicles in physiological media and the effect of a series of typical proteolytic enzymes (i.e. a-chymotrypsin, trypsin and pepsin) on empty and protein-loaded vesicles were evaluated revealing the great potential of such materials for biomedical applications.

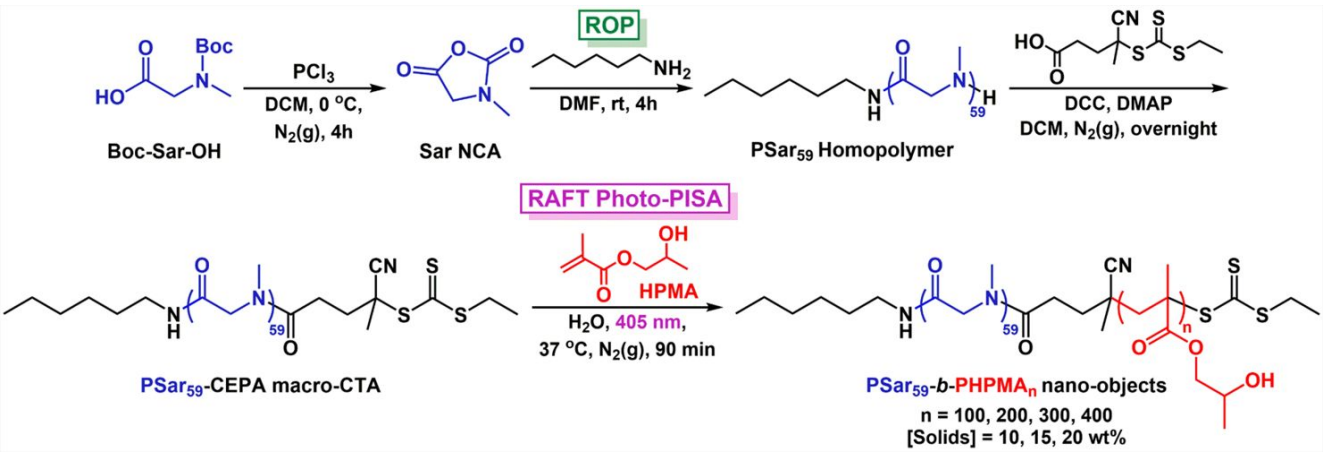

Scheme 1. Schematic illustration of the synthetic route followed for the synthesis of $PSar_{59}$-*b*-$PHPMA_n$ (n = 100, 200, 300, and 400) diblock copolymer nano-objects at [solids] = 10, 15, and 20 wt% *via* aqueous RAFT-mediated photo-PISA, using a $PSar_{59}$-based macro-CTA.

EXPERIMENTAL SECTION

Materials and methods

Materials and characterization techniques used are given in detail in the Supporting Information (SI).

Synthetic Procedures

Synthesis of sarcosine *N*-carboxyanhydride (Sar NCA). Boc-*N*-methylglycine (Boc-Sar-OH) (7.0 g, 0.037 mol) was added into a three-neck round-bottom flask and degassed under vacuum overnight. Then, 300 mL of dry DCM was distilled and the solution was left under stirring for 30 min at 0 °C. Subsequently, phosphorous trichloride (PCl_3) (4.0 mL, 0.046 mol) was diluted into 30 mL of dry DCM, added dropwise to the flask *via* a dropping funnel and the reaction was left to proceed for 4 h at 0 °C under nitrogen atmosphere. The solvent and the volatiles were removed under reduced pressure, yielding a yellowish oil as the crude reaction product. The crude product was then sublimated at 70 °C under high vacuum (10^{-5} mbar) resulting in the formation of Sar NCA crystals (3.1 g, 0.027 mol, 73%, m. p.: 103–104 °C (lit.: 102−105 °C)).[60] ^{1}H-NMR (400 MHz, DMSO-d_6): δ (ppm) 4.23 (s, 2H, C***H*****$_2$**), 2.87 (s, 3H, C***H*****$_3$**). FT-IR (neat): ν (cm^{-1}) 1848, 1761 (C=O).

Synthesis of 4-cyano-4-[(ethylsulfanylthiocarbonyl)sulfanyl] pentanoic acid (CEPA). A previously described process was followed for the synthesis of 4-cyano-4-[(ethylsulfanylthiocarbonyl)sulfanyl] pentanoic acid chain transfer agent (CEPA CTA).[61] In

particular, sodium ethanethiolate (10.0 g, 0.119 mol, 1 eq) was suspended in 500 mL of dry diethyl ether at 0 °C. Carbon disulfide (7.74 mL, 0.131 mol, 1.1 eq) was subsequently added dropwise over 10 min, resulting to the formation of a thick yellow precipitate of sodium *S*-ethyl trithiocarbonate. After 2 h of stirring at room temperature, solid iodine (15.1 g, 0.059 mol, 0.5 eq) was added to the reaction medium. After 2 h, the solution was washed three times with aqueous sodium thiosulfate (1 M), water and finally saturated NaCl solution. The organic layer was thoroughly dried over $MgSO_4$ and the crude bis-(ethylsulfanylthiocarbonyl) disulfide was then isolated by rotary evaporation (16.2 g, 0.059 mol).

A solution of bis-(ethylsulfanylthiocarbonyl) disulfide (16.2 g, 0.059 mol, 1 eq) and 4,4′-azobis(4-cyanopentanoic acid) (ACVA) (24.8 g, 0.0885 mol, 1.5 eq) in 500 mL ethyl acetate was heated at reflux for 18 h under N_2(g) atmosphere. Following rotary evaporation of the solvent, the crude CEPA CTA was isolated by flash column chromatography using silica gel as the stationary phase and 75:25 DCM-petroleum ether as the eluent. The isolated product was precipitated out of solution using hexane, leaving a yellow-light orange solid. The final product was collected and dried under reduced pressure to afford pure CEPA CTA (21.36 g, 0.081 mol, 69%). ^{1}H-NMR (400 MHz, $CDCl_3$): δ (ppm) 3.35 (q, 2H, S-C***H*****$_2$**-CH_3), 2.38-2.71 (m, 4H, C***H*****$_2$**-C***H*****$_2$**), 1.89 (s, 3H, C(CN)-C***H*****$_3$**), 1.36 (t, 3H, S-CH_2-C***H*****$_3$**). ^{13}C-NMR (100 MHz, $CDCl_3$): δ (ppm) 217.0, 177.2, 119.2, 46.5, 33.5, 31.7, 29.5, 25.0, 12.9. FT-IR (neat): ν (cm^{-1}) 2235 (C≡N), 1709 (C=O), 1073 (C=S). HRMS: m/z $[C_9H_{13}NO_2S_3+Na]^+$ calc. 286.0001 g mol^{-1}, exp. 286.0001 g mol^{-1}.

Synthesis of poly(sarcosine)$_{59}$ (PSar$_{59}$) *via* ring-opening polymerization (ROP) of Sar NCA. In a flame-dried round bottom flask, n-hexylamine (0.048 mL, 3.6×10^{-5} mol) was added, followed by distillation of 30 mL highly pure DMF. The flask was transferred to the glove box and a 10 mL

solution of Sar NCA (2.9 g, 0.0252 mol) in DMF was added and the solution was vigorously stirred at room temperature. Periodically, the solution was pumped to remove the CO_2 (g) produced during polymerization. The consumption of Sar NCA was monitored by FT-IR spectroscopy through removal of an aliquot of the solution in the glove box. Upon completion of the polymerization reaction (4 h), the final PSar homopolymer was precipitated in diethyl ether and dried under vacuum overnight (1.5 g, 83%). ^{1}H-NMR (400 MHz, D_2O): δ (ppm) 4.49-4.05 (br m, C***H₂*** of PSar backbone), 3.21 (m, 2H, CH_2-C***H₂***-NH), 3.10-2.81 (br m, C***H₃*** of PSar side chain), 1.50 (s, 2H, $(CH_2)_3$-C***H₂***-CH_2-NH), 1.29 (s, 6H, CH_3-(C***H₂***)$_3$-CH_2), 0.86 (s, 3H, C***H₃***-$(CH_2)_3$-CH_2). $M_{n,\ NMR}$ = 4,200 g mol^{-1} ($DP_{PSar,\ NMR}$ = 59). FT-IR (neat): ν (cm^{-1}) 1641 (C=O of amide). SEC (5 mM NH_4BF_4 in DMF) $M_{n,\ SEC\ RI}$ = 7,700 g mol^{-1}, $Đ_{M,\ SEC\ RI}$ = 1.08. $M_{w,\ SLS}$ = 5,500 g mol^{-1}.

Synthesis of poly(sarcosine)$_{59}$-CEPA macro-CTA ($PSar_{59}$-CEPA macro-CTA). $PSar_{59}$-CEPA macro-CTA was synthesized by dicyclohexylcarbodiimide (DCC) coupling between $PSar_{59}$ and CEPA CTA according to previously reported methods.[42, 48, 59] Poly(sarcosine) homopolymer ($M_{n,\ NMR}$ = 4,200 g mol^{-1}, $PSar_{59}$) (1 g, 2.4×10^{-4} mol, 1 eq) was dissolved in 20 mL of dry DCM. The resulting solution was then purged with N_2 (g) for 30 min. After complete dissolution, CEPA CTA (0.253 g, 9.6×10^{-4} mol, 4 eq), DCC (99 mg, 4.8×10^{-4} mol, 2 eq) and DMAP (5.9 mg, 4.8×10^{-5} mol, 0.2 eq) were added to the reaction mixture. The amide formation reaction proceeded with stirring at room temperature for 18 h under continuous N_2 (g) flow. After this period, DCC (99 mg, 4.8×10^{-4} mol, 2 eq) and DMAP (5.9 mg, 4.8×10^{-5} mol, 0.2 eq) were added for a second time to the reaction mixture and then stirred at room temperature for an additional period of 6 h under continuous N_2 (g) flow. The solution was then filtered to remove unreacted DCC and DMAP. Following rotary evaporation of DCM, the resulted $PSar_{59}$-CEPA macro-CTA was collected by precipitation into

250 mL of cold diethyl ether, redissolved in deionized water (DI) and dialyzed against DI water for 48 h (dialysis membrane MWCO = 1,000 Da). The purified $PSar_{59}$-CEPA macro-CTA was then lyophilized to give a yellowish solid as the final product (0.82 g, 1.8×10^{-4} mol, 76%). ^{1}H-NMR (400 MHz, $CDCl_3$): δ (ppm) 4.35-3.85 (br m, C***H₂*** of PSar backbone), 3.35 (q, 2H, CH_3-C***H₂***-S-(C=S)), 3.21 (m, 2H, CH_2-C***H₂***-NH), 3.10-2.85 (br m, C***H₃*** of PSar side chain), 2.69 (m, 2H, C***H₂***-(C=O)-N-CH_3), 2.52-2.35 (m, 2H, C(CN)-C***H₂***), 1.91 (s, 3H, C***H₃***-C-(CN)), 1.49 (s, 2H, $(CH_2)_3$-C***H₂***-CH_2-NH), 1.36 (t, 3H, C***H₃***-CH_2-S-(C=S)), 1.25 (d, 6H, CH_3-(C***H₂***)$_3$-CH_2), 0.88 (s, 3H, C***H₃***-$(CH_2)_3$-CH_2). SEC (5 mM NH_4BF_4 in DMF) $M_{n,\,SEC\,RI}$ = 8,300 g mol^{-1}, $Đ_{M,\,SEC\,RI}$ = 1.09.

Synthesis of $PSar_{59}$-*b*-$PHPMA_n$ diblock copolymer nano-objects by aqueous RAFT-mediated photoinitiated polymerization-induced self-assembly (photo-PISA). All photo-PISA reactions were performed in a custom-built photoreactor setup (see the Supporting Information for details). This ensured the polymerization solutions were only exposed to the light from the 400−410 nm LED source placed underneath the vials (radiant flux of 800 mW@400 mA). A typical synthetic procedure to achieve $PSar_{59}$-*b*-$PHPMA_{200}$ diblock copolymer nano-objects at 15 wt% solids content by aqueous RAFT-mediated photo-PISA is described.[42, 59] $PSar_{59}$-CEPA mCTA (20 mg, 4.4×10^{-6} mol, 1 eq) and HPMA (128 mg, 8.9×10^{-4} mol, 200 eq) were dissolved in deionized water (0.84 mL) in a sealed 15 mL scintillation vial bearing a magnetic stirrer bar. The resulting polymerization solution was degassed by purging with N_2 (g) for 15 min. The sealed vial was incubated at 37 °C with magnetic stirring under 405 nm light irradiation for 90 min to ensure full monomer conversion. After this period, the reaction mixture was exposed to air and allowed to cool to room temperature. The resulting solution of particles was then diluted ten-fold in DI water and purified by three centrifugation/resuspension cycles in DI water at 14000 rpm. ^{1}H-NMR in

methanol-d_4 and DMF SEC analyses of the pure copolymers were performed after lyophilization of an aliquot of particles. TEM, DLS and zeta potential analyses were performed on samples after dilution to an appropriate analysis concentration. ^{1}H-NMR (400 MHz, CD_3OD): δ (ppm) 5.60 (br s, O***H***), 4.47-4.10 (br m, C***H₂*** of PSar backbone), 4.03 and 3.88 (br s, C***H*** and C***H₂*** of PHPMA side chain), 3.63 (br s, C***H*** of PHPMA side chain, isomer peak), 3.10-2.89 (br m, C***H₃*** of PSar side chain), 2.23-1.75 (br m, C***H₂*** of PHPMA backbone), 1.50-0.75 (br m, C***H₃*** of PHPMA backbone and C***H₃*** of PHPMA side chain).

Encapsulation of HRP into $PSar_{59}$-*b*-$PHPMA_{400}$ vesicles by one-pot aqueous RAFT photo-PISA. For the preparation of HRP-loaded $PSar_{59}$-*b*-$PHPMA_{400}$ vesicles by aqueous photo-PISA at 10 wt% solids content, a typical synthetic protocol was followed.[57] $PSar_{59}$-CEPA mCTA (10 mg, 2.2×10^{-6} mol, 1 eq) and HPMA (128 mg, 8.9×10^{-4} mol, 400 eq) were dissolved in deionized water (1.14 mL) in a sealed 15 mL scintillation vial bearing a magnetic stirrer bar. Once homogeneous, 0.1 mL of a 200 U mL^{-1} HRP solution in DI water was added. The resulting polymerization solution was degassed by purging with N_2 (g) for 15 min. The sealed vial was incubated at 37 °C with magnetic stirring under 405 nm light irradiation for 90 min to ensure full monomer conversion. After this period, the reaction mixture was exposed to air and allowed to cool to room temperature. The resulting solution of particles was then diluted ten-fold in 100 mM PB (pH = 7.0) and purified by five centrifugation/resuspension cycles in 100 mM PB (pH = 7.0) at 14000 rpm for the removal of unreacted monomer and free HRP enzyme.

Incubation of empty and HRP-loaded $PSar_{59}$-*b*-$PHPMA_{400}$ vesicles with different proteolytic enzymes (proteases). Empty $PSar_{59}$-*b*-$PHPMA_{400}$ vesicles purified in 100 mM phosphate buffer

(PB) (pH = 7.0 for a-chymotrypsin and trypsin or pH = 1.8 for pepsin) at 10× dilution (1 wt% solids content) (2 mL) were incubated with either 25 mg mL^{-1} a-CT (pH = 7.0), 25 mg mL^{-1} trypsin (pH = 7.0) or 25 mg mL^{-1} pepsin (pH = 1.8) solutions (0.2 mL) at 37 °C. Aliquots were taken over a period of 72 h and samples were analyzed by DLS, DMF SEC and dry-state TEM imaging to determine the effect of different proteases on the characteristics of particles.

HRP-loaded $PSar_{59}$-*b*-$PHPMA_{400}$ vesicles purified in 100 mM PB (pH = 7.0 for a-CT and trypsin) at 10× dilution (1 wt% solids content) (2 mL) were incubated with either 100 mM PB (pH = 7.0), 25 mg mL^{-1} a-CT or trypsin (pH = 7.0) solutions (0.2 mL) at 37 °C for a period of 72 h. Aliquots were taken at 18 h and 72 h and the relative activities of particles were assessed by kinetic colorimetric analysis using a plate reader. For the free HRP, 2 U mL^{-1} solutions in 100 mM PB (pH = 7.0) (2 mL) were incubated with either 100 mM PB (pH = 7.0), 25 mg mL^{-1} a-CT or trypsin (pH = 7.0) solutions (0.2 mL) at 37 °C for a period of 72 h. Aliquots were taken at 18 h and 72 h and the relative activities of free HRP solutions were assessed in an identical manner. Pepsin was not used in case of HRP-loaded vesicles due to significant difference in optimum pH range of the two enzymes.

Kinetic colorimetric analyses for determination of activity of HRP-loaded $PSar_{59}$-*b*-$PHPMA_{400}$ vesicles in presence of different proteases. Purified HRP-loaded $PSar_{59}$-*b*-$PHPMA_{400}$ vesicles incubated with either PB, a-CT or trypsin at 20× dilution (0.5 wt% solids content) in 100 mM PB (pH = 7.0) (120 μL) were diluted with 100 mM PB (pH = 7.0) (40 μL) in a 96-well plate microwell. *O*-dianisidine (4 mM, 20 μL) was then added. Finally, a 35 wt% aqueous solution of hydrogen peroxide (20 μL) was added and the change in absorbance at λ = 492 nm was recorded every minute for a period of 60 min using a plate reader. In a similar process, the free

HRP solutions incubated with either PB, a-CT or trypsin at 1 U mL^{-1} in 100 mM PB (pH = 7.0) (20 μL) were diluted with 100 mM PB (pH = 7.0) (140 μL) in a 96-well plate microwell. *O*-dianisidine (4 mM, 20 μL) was then added. Finally, a 35 wt% aqueous solution of hydrogen peroxide (20 μL) was added and the change in absorbance was monitored in an identical manner. All measurements were performed in quadruplicate.

Colloidal stability studies of $PSar_{59}$-*b*-$PHPMA_{400}$ vesicles in physiological media. To assess the colloidal stability of empty $PSar_{59}$-*b*-$PHPMA_{400}$ vesicles (prepared at [solids] = 10 wt%) and their interaction with complex physiological media, a typical protocol was followed.[62] FBS and cell growth medium were first incubated at 37 °C for 15 min. Purified $PSar_{59}$-*b*-$PHPMA_{400}$ vesicles were suspended in DI water at a final concentration of 1 wt% prior to mixing with FBS or cell growth medium. Then, 80 μL of 1 wt% vesicles were dispersed in either 10 mL DI water or cell growth medium or 10 mL of 1:9 FBS:DI H_2O solution, with gentle agitation. The resulting particle solutions were incubated at 37 °C and D_h changes of vesicles were monitored by DLS over a period of 72 h.

RESULTS AND DISCUSSION

Synthesis and characterization of poly(sarcosine)$_{59}$ ($PSar_{59}$) homopolymer. The first step for the preparation of PSar homopolymer involved the synthesis of the corresponding *N*-carboxyanhydride of sarcosine (Sar NCA). This was achieved by cyclization reaction of *N*-Boc-protected sarcosine using PCl_3 as chlorinating agent for the formation of Sar NCA ring molecule (Scheme 1). The reaction was completed in 4 h as evidenced by FT-IR spectroscopy (Figure S2, SI). The appearance of two characteristic peaks at 1761 and 1848

cm^{-1} are indicative of the ν(C=O) vibrations of the Sar NCA ring. The crude product was purified by sublimation *in vacuuo* resulting in the formation of Sar NCA crystals. The successful synthesis and purification of Sar NCA was confirmed by ^{1}H-NMR spectroscopy in DMSO-d_6 (Figure S1A, SI). Although the "Fuchs-Farthing" method is considered the standard approach for the synthesis of amino acid NCAs (i.e. use of phosgene or derivatives at elevated temperatures), the alternative mild synthetic procedure followed herein resulted in highly pure final product of Sar NCA at high yield.

Next, ω-telechelic PSar homopolymer was synthesized *via* living ring-opening polymerization (ROP) of Sar NCA. The polymerization reaction proceeded under high vacuum at room temperature for 4 h using n-hexylamine as the initiator and DMF as the solvent, and was terminated by precipitation in diethylether (Scheme 1). Monitoring of the ROP kinetics was carried out *via* FT-IR spectroscopy as evidenced by the disappearance of the NCA peaks (1761 and 1848 cm^{-1}) and the gradual appearance of a sharp peak at 1641 cm^{-1} attributed to the ν(C=O) vibration of the formed poly(peptoid) amide bonds (Figure S2, SI). SEC analysis in DMF with 5 mM NH_4BF_4 was carried out to get a rough molecular weight estimate of the homopolymer as PMMA can be poor standard for PSar, while it revealed a narrow monomodal molecular weight distribution peak of low dispersity ($M_{n,\ SEC\ RI}$ = 7,700 g mol^{-1}, $Đ_{M\ RI}$ = 1.08) (Figure 1B).[60] ^{1}H-NMR spectroscopy in D_2O was used for the determination of the average degree of polymerization (DP) of the final purified PSar by comparing the integral ratio of the peak corresponding to –CH_3 group of hexylamine at 0.86 ppm ($I_{0.86\ ppm}$ = 3.00) to the peak of –CH_3 groups of PSar backbone at 2.81-3.10 ppm ($I_{2.81\text{-}3.10\ ppm}$ = 177.25) (ca. DP_{PSar} = 59, $M_{n,\ NMR}$ = 4,200 g mol^{-1}) (Figure S1B, SI). Analysis of static and dynamic light scattering over a range of scattering lengths (10.7

$\leq q \leq 23.0$ μm^{-1}) was used to estimate the weight-average molecular weight and intensity-weighted hydrodynamic radius of $PSar_{59}$ in DI water $\left(M_w = (5.50 \pm 0.09) \times 10^3 \text{ Da}; \langle R_h \rangle_Z = (1.95 \pm 0.03) \text{ nm}\right)$ (Figure S3, SI). The mutual consistency of these two measurements was then verified by reference to an empirical formula published previously by Weber et al.[60]

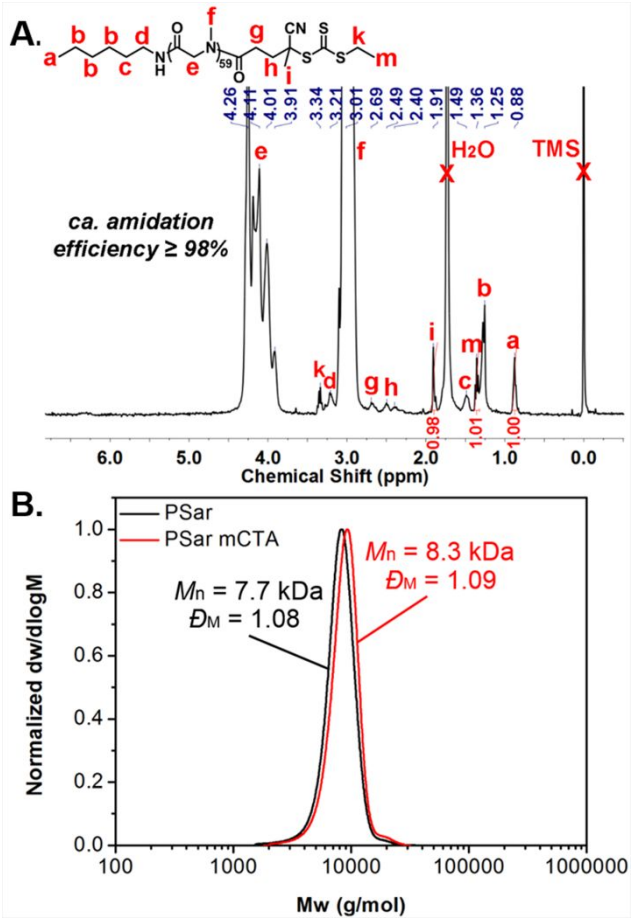

Figure 1. (A) ^{1}H-NMR spectrum of $PSar_{59}$-CEPA macro-CTA in $CDCl_3$. (B) Normalized SEC RI molecular weight distributions for $PSar_{59}$ homopolymer (black trace) and $PSar_{59}$-CEPA macro-CTA (red trace), along with the corresponding M_n and $Đ_M$ values. M_n and $Đ_M$ values were calculated from PMMA standards using 5 mM NH_4BF_4 in DMF as the eluent.

Aqueous RAFT-mediated photoinitiated polymerization-induced self-assembly (photo-PISA) of $PSar_{59}$-*b*-$PHPMA_n$ diblock copolymer nano-objects. In order to conduct aqueous RAFT-mediated photo-PISA reactions using $PSar_{59}$ as the hydrophilic steric stabilizer, a small molecule CTA (CEPA CTA) suitable for methacrylate monomers was introduced to the PSar chain ends to afford a PSar-based macro-CTA. This was achieved through amide bond formation between the acid-functionalized CEPA CTA and the sterically accessible amino end group of PSar by DCC coupling chemistry under dry conditions (Scheme 1). Quantitative amidation efficiency (≥98%) was calculated from ^{1}H-NMR spectroscopy in chloroform-*d* by comparing the integral ratio of the peak corresponding to $–CH_3$ group of hexylamine at 0.88 ppm ($I_{0.88\ ppm}$ = 1.00) to the peak of $–CH_3$ group of CTA at 1.91 ppm ($I_{1.91\ ppm}$ = 0.98) (ca. amidation efficiency (%) = ($I_{1.91\ ppm}/I_{0.88\ ppm}$)×100, Figure 1A). Based on ^{1}H-NMR analysis, there is approximately 2% of non-fuctionalized $PSar_{59}$ homopolymer that is not separated from $PSar_{59}$-CEPA macro-CTA as they both precipitate from diethyl ether. SEC analysis of the purified and lyophilized $PSar_{59}$ macro-CTA in 5 mM NH_4BF_4 in DMF revealed the successful attachment of CEPA, as judged by the small increase of molecular weight compared to $PSar_{59}$ and the characteristic absorbance of the trithiocarbonate group of the macro-CTA peak at λ = 309 nm ($M_{n,\ SEC\ RI}$ = 8,300 g mol^{-1}, $Đ_{M\ RI}$ = 1.09) (Figure 1B).

Subsequently, the prepared water-soluble $PSar_{59}$ macro-CTA was chain-extended under RAFT dispersion PISA conditions using the well-documented water-miscible monomer 2-hydroxypropyl methacrylate (HPMA) (mixture of 2-hydroxypropyl methacrylate - 75 mol % and 2-hydroxyisopropyl methacrylate – 25 mol%) for the formation of the water-insoluble core-forming block. Aqueous RAFT-mediated photo-PISA reactions of HPMA for the fabrication of $PSar_{59}$-*b*-$PHPMA_n$ diblock copolymer nano-objects were carried out under 405

nm visible-light irradiation (radiant flux of 800 mW@400 mA) at 37 °C (N_2 atmosphere) in the absence of a photoinitiator or catalyst (Scheme 1). As an initial step, the required photo-PISA reaction time to ensure complete monomer conversions was determined *via* kinetic study of a $PSar_{59}$-*b*-$PHPMA_{400}$ system at 10 wt% total solids content. Aliquots were withdrawn from the polymerization mixture every 5 min and samples were analysed by ^{1}H-NMR spectroscopy in methanol-d_4 for monomer conversion calculation and SEC analysis using 5 mM NH_4BF_4 in DMF as the eluent. As shown in Figure 2A, the photo-PISA reaction followed pseudo-first-order kinetics separated into two regimes with quantitative monomer conversion (>99%) achieved after 90 min of irradiation time. Based on the semilogarithmic plot, the first regime from 0 to 25 min corresponds to growing solvent-soluble $PSar_{59}$-*b*-$PHPMA_n$ chains, while for the second regime a significant increase in polymerization rate typically occurring in a PISA process was observed after approximately 25 min ascribed to a monomer conversion of 36.5% that is attributed to the onset of particle micellization resulting in a relatively high local HPMA concentration.[33, 63] SEC monitoring during the kinetic study revealed the linear evolution of M_n values with conversion and verified the controlled character of the photo-PISA process, while $Đ_M$ values remained relatively low with progression of conversion ($Đ_M$ max = 1.50), given that a high DP of PHPMA was targeted in this case (Figure 2B).

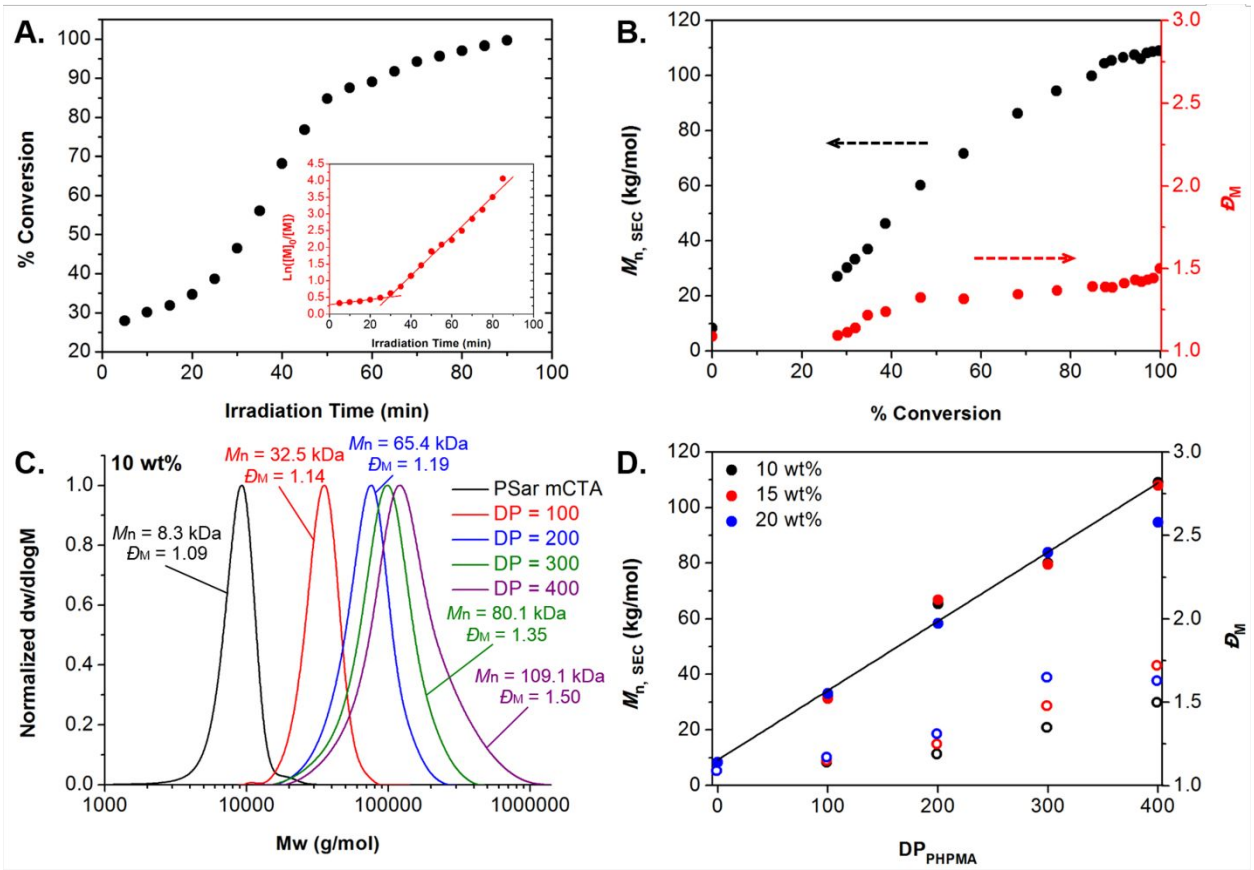

Figure 2. (A) Polymerization kinetics for aqueous RAFT-mediated photo-PISA of HPMA using $PSar_{59}$-CEPA as the macro-CTA at [solids] = 10 wt% (target DP_{PHPMA} = 400) (inset: $\ln([M]_0/[M])$ *versus* irradiation time kinetic plot). (B) Evolution of number-average molecular weight (M_n) and molar mass distribution ($Đ_M$) values with monomer conversion for aqueous RAFT-mediated photo-PISA of HPMA using $PSar_{59}$-CEPA as the macro-CTA at [solids] = 10 wt% (target DP_{PHPMA} = 400). (C) Normalized SEC RI molecular weight distributions for $PSar_{59}$-CEPA macro-CTA (black trace) and $PSar_{59}$-*b*-$PHPMA_n$ diblock copolymers (n = 100 - red trace, 200 - blue trace, 300 - green trace, and 400 - purple trace) at [solids] = 10 wt%, along with their corresponding M_n and $Đ_M$ values. (D) Evolution of M_n (filled circles) and $Đ_M$ (empty circles) values calculated from SEC RI analysis with increasing target DP of PHPMA for $PSar_{59}$-*b*-$PHPMA_n$ diblock copolymers prepared *via* aqueous RAFT-mediated photo-PISA at [solids] = 10, 15, and 20 wt%. In all cases M_n and $Đ_M$ values were calculated from PMMA standards using 5 mM NH_4BF_4 in DMF as the eluent.

Next, a series of aqueous photo-PISA reactions under the same mild polymerization conditions were carried out for 90 min for the development of $PSar_{59}$-*b*-$PHPMA_n$ diblock copolymer nano-objects of different morphologies by targeting various DPs of the core-forming PHPMA block (DP_{PHPMA} = 100, 200, 300, and 400) and total solids concentrations ([solids] = 10, 15, and 20 wt%). In all cases complete monomer conversion (≥98%) was achieved in 90 min of irradiation time, as determined by ^{1}H-NMR spectroscopic analysis in methanol-d_4 of the crude copolymer samples (Table S1, SI). The $PSar_{59}$-*b*-$PHPMA_n$ nano-object samples were purified by consecutive centrifugation-resuspension cycles in DI water for the removal of unreacted monomer (Figure S4, SI). Based on SEC analysis of lyophilized samples using 5 mM NH_4BF_4 in DMF as the eluent, the well-controlled character of photo-PISA reactions at different solids content was revealed. Specifically, in all cases symmetrical monomodal molecular weight distributions were observed shifting linearly toward higher molecular weight (M_n) values upon increasing the DP of PHPMA with no apparent trace of bimolecular termination (Figures 2C and S5, SI). Based on SEC RI chromatograms of $PSar_{59}$-*b*-$PHPMA_n$ diblock copolymers, a low molecular weight peak that corresponds to non-separated and non-functionalized $PSar_{59}$ homopolymer (~4–5% of $PSar_{59}$-CEPA macro-CTA trace in all cases, ca. 2% from ^{1}H-NMR analysis) is observed, but since it doesn't contribute to RAFT-mediated chain-extensions of PHPMA or affect the overall nano-object characteristics it was not taken into consideration for the calculation of M_n and $Đ_M$ values of the main $PSar_{59}$-*b*-$PHPMA_n$ diblock copolymer peak in each case (Figure S6, SI). Importantly, for a series of samples with specified block copolymer composition (i.e. same target DP of PHPMA) at different total solids concentration ranging from 10-20 wt%, comparable M_n values were measured throughout. Low dispersity values were calculated

when targeting shorter PHPMA blocks with increasing $Đ_M$ upon gradually increasing either the DP of the core-forming block or the total solids content (Figure 2D and Table S1). This behavior of M_n and $Đ_M$ values' progression is typical for dispersion PISA systems.

Exhaustive dry-state stained transmission electron microscopy (TEM) imaging along with dynamic light scattering (DLS) and zeta-potential analyses were used for the characterization of $PSar_{59}$-*b*-$PHPMA_n$ block copolymer nano-objects in solution (Figures S7-S18 and Table S2, SI). Morphologies evolving from spherical micelles (S - spheres) to worm-like micelles (W - worms) and vesicular nanostructures (V - vesicles) along with intermediate mixed morphologies were observed upon targeting higher DPs of the core-forming PHPMA block and solids concentration. In particular, a mixture of spheres and short worms was obtained in the case of $PSar_{59}$-*b*-$PHPMA_{100}$ diblock copolymer system at [solids] = 10 and 15 wt%, while a pure phase of worms could be accessed for the same block copolymer composition at 20 wt%, as sphere-sphere fusion is more favorable at higher solids content. This was evident macroscopically by the formation of a clear free-standing gel in the reaction vial after photo-PISA. In all three cases, low hydrodynamic diameter (D_h) and polydispersity (PD) values were measured ranging from 29 - 47 nm and 0.06 - 0.16, respectively, accompanied by narrow particle size distributions. Aqueous photo-PISA reaction targeting DP_{PHPMA} = 200 at [solids] = 10 wt% lead to the formation of a mixed phase of all three morphologies (S+W+V), due to coexistence of two particle populations initially indicated by DLS analysis and shown by TEM imaging. A mixture of worm-like micelles and spherical vesicles was formed for the same DP of PHPMA at [solids] = 15 and 20 wt%. In these cases D_h and PD values were found to be relatively higher (D_h = 200 - 500 nm and PD = 0.13 - 0.36) compared to the ones corresponding to $PSar_{59}$-*b*-$PHPMA_{100}$ due to existence of mixed morphologies of small and

larger nano-objects. For DP_{PHPMA} = 300 at [solids] = 10 wt%, an intermediate morphology between worms and vesicles was observed, while pure vesicular morphologies were formed at higher solids concentrations for the same target DP of PHPMA. Interestingly, a pure phase of long tubular vesicles was detected for $PSar_{59}$-*b*-$PHPMA_{300}$ at [solids] = 15 wt% of average D_h = 1360 nm and PD = 0.22 showing great promise for nanocarrier design applications as it is proven that non-spherical particles exhibit longer circulation times *in vivo* and could be more easily uptaken by cells.[64] In the case of 20 wt% total solids content for DP_{PHPMA} = 300, micron-sized oligolamellar vesicles of relatively low PD were detected by dry-state TEM imaging. More importantly, pure spherical and elongated unilamellar vesicles with D_h = 321 nm and narrow particles' size distribution were obtained for $PSar_{59}$-*b*-$PHPMA_{400}$ formed at 10 wt% that could potentially be utilized for nanoreactor development. Finally, a mixture of elongated tubular and multilamellar vesicles was formed in case of DP_{PHPMA} = 400 at [solids] = 15 wt%, while an intriguing morphology of large perforated vesicles with D_h = 1515 nm and PD = 0.22 was observed at 20 wt% solids content. The unusual higher-order vesicular morphologies observed at exceedingly high DPs and wt% of PHPMA are mainly attributed to the development of significant hydrophobic interactions between the PHPMA cores and the short hydrophobic segment of hexylamine located in front of the hydrophilic stabilizer block of PSar that could promote further entanglement of the polymer chains and formation of loops potentially aiding the fabrication of flower-like nanostructures.

Based on the obtained results, a detailed phase diagram was constructed to summarize the observed nano-object morphologies of different $PSar_{59}$-*b*-$PHPMA_n$ formulations developed upon varying DP_{PHPMA} and [solids] (wt%) and to allow for the facile reproducibility of our findings (Figure 3). Importantly, in all $PSar_{59}$-*b*-$PHPMA_n$ nano-object formulations, zeta-

potential values of around 0 mV (zeta-potential = -0.15 – +0.07 mV) were measured from microelectrophoretic analysis at neutral pH that were independent of pH variations from acidic (pH = 4.0) to basic (pH = 9.0) values (Table S2, SI), revealing the absence of net charges on the outer surface of particles and their promising "stealth" character as they can prevent the activation of the immune system upon insertion to the body.

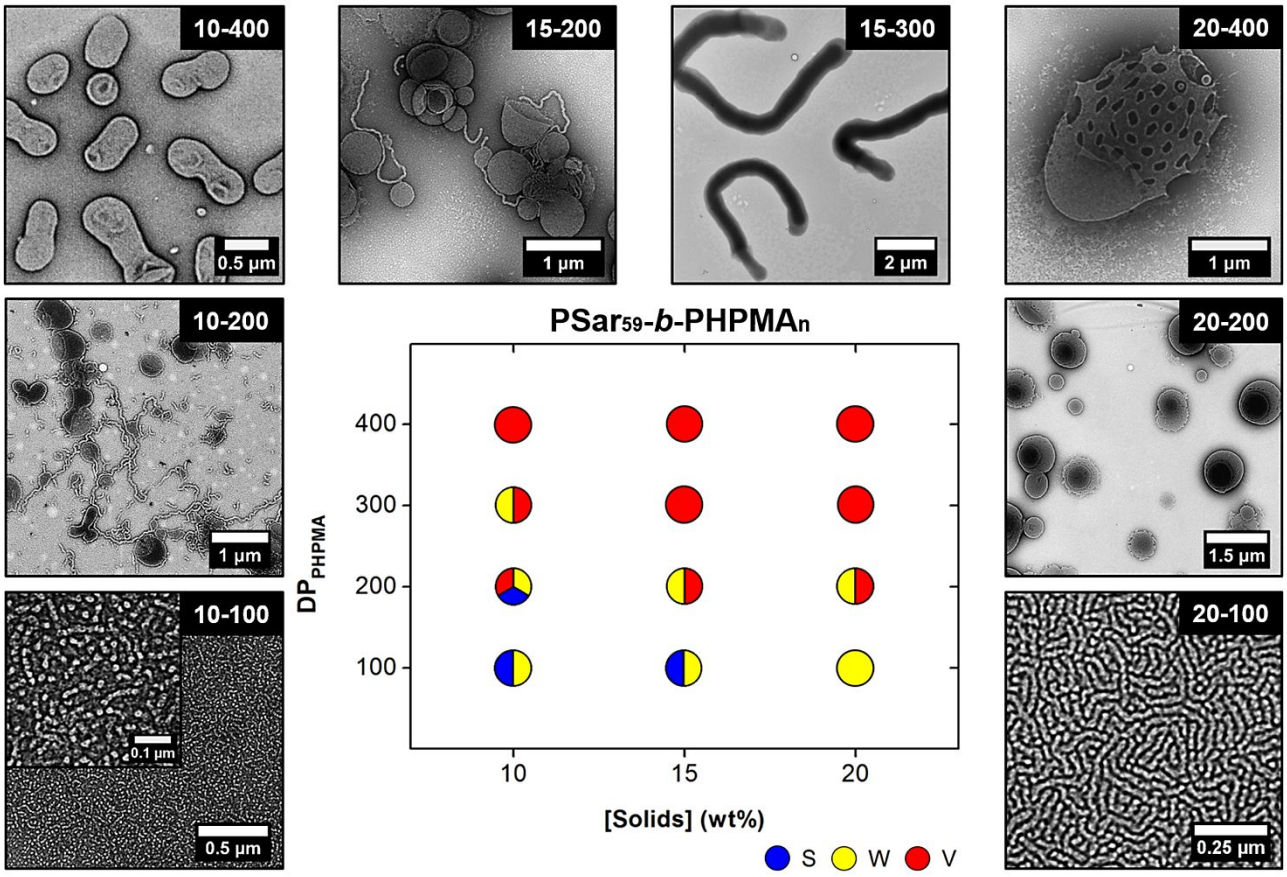

Figure 3. Detailed morphologies diagram for $PSar_{59}$-*b*-$PHPMA_n$ diblock copolymer nano-objects prepared *via* aqueous RAFT-mediated photo-PISA of HPMA by varying the total solids content and DP of PHPMA, along with representative dry-state TEM images of different formulations, stained with 1 wt% uranyl acetate (UA) solution. Key: S – spherical micelles (blue), W – worm-like micelles (yellow), V – vesicles (red).

Colloidal stability of $PSar_{59}$-*b*-$PHPMA_{400}$ unilamellar vesicles and resistance against degradation by proteolytic enzymes. Based on the constructed morphologies diagram, the developed $PSar_{59}$-*b*-$PHPMA_{400}$ unilamellar vesicles formed at 10 wt% solids as a pure morphology were isolated and their potential use for nanoreactor fabrication and future *in vitro* and *in vivo* studies was explored. Additionally, the resistance of both empty and enzyme-loaded vesicles against a series of different proteases was also assessed.

First, the colloidal stability of empty $PSar_{59}$-*b*-$PHPMA_{400}$ vesicles in a range of complex media (i.e. DI water, fetal bovine serum (FBS) and cell culture medium) was evaluated, by monitoring the D_h changes over time using DLS upon incubation at 37 °C for a total time period of 72 h (Figure S19, SI). Not surprisingly, the average size of vesicles in DI water didn't change significantly over extended incubation periods ranging from 340 to 380 nm. In the case of vesicles incubated in aqueous FBS solution, a negligible D_h increase to 405 nm was observed after 24 h of incubation time which was more evident after 72 h (D_h = 448 nm), indicating slow time-dependent agglomeration of particles with blood components such as serum proteins (e.g. albumins and globulins).[62] On the contrary, for empty vesicles incubated in cell growth medium, a minor D_h decrease was observed after 24 h of incubation time to 220 nm while their size remained constant for the rest of the study. Overall, the obtained results revealed the good colloidal properties of $PSar_{59}$-*b*-$PHPMA_{400}$ vesicles in physiological media for prolonged time periods.

Additionally, to further assess the effect of common proteolytic enzymes on the PSar poly(peptoid) corona of $PSar_{59}$-*b*-$PHPMA_{400}$ vesicles and the potential ability of the formed nanostructures to act as protective cages of delicate enzymes for development of vesicular nanoreactors, particle solutions at 10-fold dilution from original concentration were incubated

with a series of proteases (i.e. a-chymotrypsin, trypsin and pepsin) at 37 °C and appropriate pH for a period of 72 h (Figure 4). Structural and molecular characteristics' changes of empty $PSar_{59}$-*b*-$PHPMA_{400}$ were monitored by DLS and SEC analyses and dry-state TEM imaging for determination of the ability of hydrophilic and non-ionic $PSar_{59}$ stabilizer block to resist proteolysis. Size variations of the vesicle solutions incubated with either a-chymotrypsin (a-CT) or trypsin at pH = 7.0 and pepsin at pH = 1.8 were measured by DLS analysis (Figure 4A). In case of a-CT and trypsin, the overall dimensions of particles remained constant in the range of 305-335 nm for the total incubation period of 72 h, while for pepsin a slight size increase to 380 nm was monitored after 24 h mainly attributed to the exceedingly low pH level of the solution affecting the measurements upon extended incubation time periods. Near-identical SEC molecular weight distributions were recorded for lyophilized samples in all three cases with M_n and $Đ_M$ values being similar to those of empty $PSar_{59}$-*b*-$PHPMA_{400}$ diblock copolymers formed by aqueous photo-PISA at 10 wt% (Figure 4B), showing no apparent peptoid bond hydrolysis taking place. Dry-state TEM imaging of empty vesicles after 72 h of incubation time with each protease proved that no changes in shape and size of nano-objects occurred showing their excellent stability toward biodegradation from various proteolytic enzymes (Figures 4C and S20, SI).

Based on these findings, the ability of $PSar_{59}$-*b*-$PHPMA_{400}$ vesicles to protect other sensitive hydrophilic enzymes from proteolysis by encapsulation in their inner aqueous lumen compared to free enzymes was further investigated. Horseradish peroxidase (HRP) was selected as a model enzyme for encapsulation into $PSar_{59}$-*b*-$PHPMA_{400}$ vesicles *via* a one-pot photo-PISA methodology previously described by our group.[57-59] In these studies, it was shown that such enzymes could tolerate photo-PISA reaction conditions, retain activity and communicate with the

external aqueous environment by passive diffusion of small molecules through the semipermeable and relatively hydrated PHPMA membrane of vesicles providing a read-out of permeability. Indeed, control experiments of either purging a HRP solution with N_2 (g) for 15 min or exposure to 405 nm irradiation for 90 min after N_2 (g) bubbling showed no loss of enzyme activity as compared to the untreated enzyme (Figure S21, SI). Purified HRP-loaded vesicular nanoreactors and free HRP were incubated with either a-CT or trypsin at pH = 7.0 for 72 h, and their relative activities were determined by colorimetric assays at λ = 492 nm over time and were normalized against control experiments of HRP-loaded vesicles and free enzyme incubated solely with phosphate buffer at pH = 7.0 in absence of proteases. It should be noted that pepsin was not used for incubation of HRP-loaded vesicles as the optimum pH ranges of the two enzymes differ significantly. As shown in Figure 4D, quantitative retention of activity was achieved in case of HRP-loaded vesicles after 18 and 72 h of incubation time with either a-CT (96%) or trypsin (92%). On the contrary, a significant loss of activity of 29.2% for a-CT and 41% for trypsin was noticed in case of free HRP attributed to gradual enzyme degradation from the different proteases after 18 h. An additional activity decrease to 54.9% for a-CT and 32.9% for trypsin was measured for the free enzyme solution after 72 h, clearly showing the robust nature and protective character of PSar-based vesicles toward other encapsulated biomolecules.

Importantly, when performing the described studies to determine the resistance against proteolytic degradation of purified empty and HRP-loaded PEG_{113}-*b*-$PHPMA_{400}$ unilamellar vesicles of similar size and overall characteristics previously developed by our group,[42] an near-identical retention of enzyme activity was observed in the case of HRP-loaded vesicles after 18 and 72 h of incubation time with either a-CT or trypsin. However, a significant D_h and PD increase was monitored in the case of empty PEG_{113}-*b*-$PHPMA_{400}$ unilamellar vesicles after 18 h of incubation

time with different proteases (a-CT, trypsin or pepsin), as judged by DLS analysis, mainly attributed to the enhanced protein-induced particle aggregation that occurs in this case after a certain incubation period (Figure S22, SI).

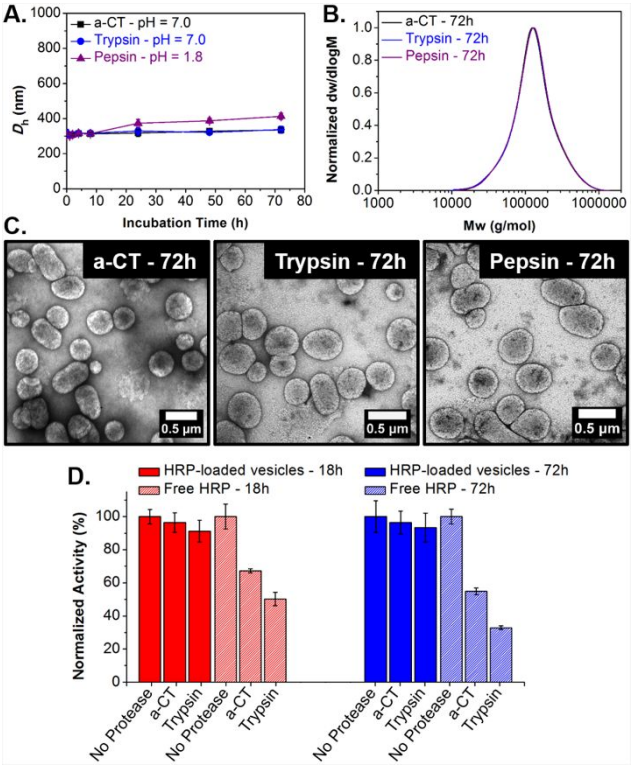

Figure 4. (A) Monitoring of hydrodynamic diameter (D_h) changes of empty $PSar_{59}$-*b*-$PHPMA_{400}$ vesicles in 100 mM PB upon incubation with a-CT (pH = 7.0), trypsin (pH = 7.0) or pepsin (pH = 1.8) at 37 °C for 72 h (the error bars show the standard deviation from five repeat measurements). (B) Normalized SEC RI molecular weight distributions for $PSar_{59}$-*b*-$PHPMA_n$ diblock copolymers after incubation with a-CT (pH = 7.0), trypsin (pH = 7.0) or pepsin (pH = 1.8) at 37 °C for 72 h. M_n and $Đ_M$ values were calculated from PMMA standards using 5 mM NH_4BF_4 in DMF as the eluent. (C) Representative dry-state TEM images of empty $PSar_{59}$-*b*-$PHPMA_{400}$ vesicles after incubation with a-CT (pH = 7.0), trypsin (pH = 7.0) or pepsin (pH = 1.8) for 72 h, stained with 1 wt% UA. (D) Normalized relative activities of HRP-loaded $PSar_{59}$-*b*-$PHPMA_{400}$ vesicles and free HRP after incubation with a-CT or trypsin at 37 °C for 18 h (red) and 72 h (blue) (the error shows the standard deviation from four repeat measurements). The normalized relative activities are defined as the ratio between the

absorbance of the samples and the absorbance of untreated HRP-loaded vesicles or free HRP, respectively, at the end point of the enzymatic assay (end point = 30 min, λ = 492 nm).

CONCLUSIONS

To conclude, we demonstrate an efficient methodology for the fabrication of poly(peptoid)-based block copolymer nano-objects with predictable morphologies at high concentrations by combining living NCA ROP and aqueous RAFT-mediated photo-PISA. In particular, poly(sarcosine) was utilized as a novel hydrophilic stabilizer block for controlled RAFT chain-extensions of a methacrylate monomer able to undergo PISA under aqueous dispersion polymerization conditions targeting different DPs of the core-forming block and total solids concentrations. A diverse set of nano-object morphologies including higher-order structures was obtained, as evidenced by the construction of a phase diagram. The colloidal stability of single phase vesicles and their ability to encapsulate hydrophilic enzymes protecting them from proteolysis were thoroughly assessed and compared to their PEG-based counterparts, showing great promise for use of the developed materials in various biomedical applications. Our findings circumvent the current limitations of conventional block copolymer self-assembly techniques, such as dilute conditions and multiple laborious post-polymerization processing and purification steps for targeting certain morphologies, underlining the potential of poly(sarcosine) as an alternative corona-forming polymer to PEG-derived polymers for fabrication of PISA nano-objects with bio-relevant character.

ASSOCIATED CONTENT

Supporting Information

The Supporting Information is available free of charge on the ACS Publications website at DOI: 10.1021/acs.bio-mac.xbxxxxx.

Materials and characterization methods, additional NMR, FT-IR, SEC and DLS data, additional dry-state TEM images, HRP control experiments and colloidal stability results.

AUTHOR INFORMATION

Corresponding Authors

*Email: nikolaos.hadjichristidis@kaust.edu.sa

*Email: r.oreilly@bham.ac.uk

Author Contributions

The manuscript was written through contributions of all authors. All authors have given approval to the final version of the manuscript.

Notes

The authors declare no competing financial interest.

ACKNOWLEDGEMENTS

This work was supported by the ERC (grant number 615142), EPSRC and King Abdullah University of Science and Technology (KAUST).

REFERENCES

1. Knop, K.; Hoogenboom, R.; Fischer, D.; Schubert, U. S., Poly(ethylene glycol) in Drug Delivery: Pros and Cons as Well as Potential Alternatives. *Angew. Chem. Int. Ed.* **2010,** 49, (36), 6288-6308.
2. Jokerst, J. V.; Lobovkina, T.; Zare, R. N.; Gambhir, S. S., Nanoparticle PEGylation for imaging and therapy. *Nanomedicine* **2011,** 6, (4), 715-728.
3. Cui, S.; Pan, X.; Gebru, H.; Wang, X.; Liu, J.; Liu, J.; Li, Z.; Guo, K., Amphiphilic star-shaped poly(sarcosine)-block-poly(ε-caprolactone) diblock copolymers: one-pot synthesis, characterization, and solution properties. *J. Mater. Chem. B* **2017,** 5, (4), 679-690.
4. Veronese, F. M.; Pasut, G., PEGylation, successful approach to drug delivery. *Drug Discov. Today* **2005,** 10, (21), 1451-1458.
5. Turecek, P. L.; Bossard, M. J.; Schoetens, F.; Ivens, I. A., PEGylation of Biopharmaceuticals: A Review of Chemistry and Nonclinical Safety Information of Approved Drugs. *J. Pharm. Sci.* **2016,** 105, (2), 460-475.
6. Jo, S.; Park, K., Surface modification using silanated poly(ethylene glycol)s. *Biomaterials* **2000,** 21, (6), 605-616.
7. Fruijtier-Pölloth, C., Safety assessment on polyethylene glycols (PEGs) and their derivatives as used in cosmetic products. *Toxicology* **2005,** 214, (1), 1-38.
8. Wang, Z.; Song, J.; Zhang, S.; Xu, X.-Q.; Wang, Y., Formulating Polyethylene Glycol as Supramolecular Emulsifiers for One-Step Double Emulsions. *Langmuir* **2017,** 33, (36), 9160-9169.
9. Lee, Y.-A.; Kim, Y.-H.; Kim, B.-J.; Jung, M.-S.; Auh, J.-H.; Seo, J.-T.; Park, Y.-S.; Lee, S.-H.; Ryu, B.-Y., Cryopreservation of Mouse Spermatogonial Stem Cells in Dimethylsulfoxide and Polyethylene Glycol1. *Biol. Reprod.* **2013,** 89, (5), 109, 1-9.
10. Harris, J. M.; Chess, R. B., Effect of pegylation on pharmaceuticals. *Nat. Rev. Drug Discovery* **2003,** 2, 214-221.
11. Ishida, T.; Harada, M.; Wang, X. Y.; Ichihara, M.; Irimura, K.; Kiwada, H., Accelerated blood clearance of PEGylated liposomes following preceding liposome injection: Effects of lipid dose and PEG surface-density and chain length of the first-dose liposomes. *J. Controlled Release* **2005,** 105, (3), 305-317.
12. Garay, R. P.; El-Gewely, R.; Armstrong, J. K.; Garratty, G.; Richette, P., Antibodies against polyethylene glycol in healthy subjects and in patients treated with PEG-conjugated agents. *Expert Opin. Drug Deliv.* **2012,** 9, (11), 1319-1323.
13. Deng, Y.; Zou, T.; Tao, X.; Semetey, V.; Trepout, S.; Marco, S.; Ling, J.; Li, M.-H., Poly(ε-caprolactone)-block-polysarcosine by Ring-Opening Polymerization of Sarcosine N-Thiocarboxyanhydride: Synthesis and Thermoresponsive Self-Assembly. *Biomacromolecules* **2015,** 16, (10), 3265-3274.
14. Hu, Y.; Hou, Y.; Wang, H.; Lu, H., Polysarcosine as an Alternative to PEG for Therapeutic Protein Conjugation. *Bioconjugate Chem.* **2018,** 29, (7), 2232-2238.
15. Pelegri-O'Day, E. M.; Lin, E.-W.; Maynard, H. D., Therapeutic Protein–Polymer Conjugates: Advancing Beyond PEGylation. *J. Am. Chem. Soc.* **2014,** 136, (41), 14323-14332.
16. Zhang, H.; Grinstaff, M. W., Recent Advances in Glycerol Polymers: Chemistry and Biomedical Applications. *Macromol. Rapid Commun.* **2014,** 35, (22), 1906-1924.
17. Hoogenboom, R., Poly(2-oxazoline)s: A Polymer Class with Numerous Potential Applications. *Angew. Chem. Int. Ed.* **2009,** 48, (43), 7978-7994.
18. Liarou, E.; Varlas, S.; Skoulas, D.; Tsimblouli, C.; Sereti, E.; Dimas, K.; Iatrou, H., Smart polymersomes and hydrogels from polypeptide-based polymer systems through α-amino acid N-

carboxyanhydride ring-opening polymerization. From chemistry to biomedical applications. *Prog. Polym. Sci.* **2018,** 83, 28-78.
19. Secker, C.; Brosnan, S. M.; Luxenhofer, R.; Schlaad, H., Poly(α-Peptoid)s Revisited: Synthesis, Properties, and Use as Biomaterial. *Macromol. Biosci.* **2015,** 15, (7), 881-891.
20. Gangloff, N.; Ulbricht, J.; Lorson, T.; Schlaad, H.; Luxenhofer, R., Peptoids and Polypeptoids at the Frontier of Supra- and Macromolecular Engineering. *Chem. Rev.* **2016,** 116, (4), 1753-1802.
21. Mudd, S. H.; Ebert, M. H.; Scriver, C. R., Labile methyl group balances in the human: The role of sarcosine. *Metabolism* **1980,** 29, (8), 707-720.
22. Weber, B.; Seidl, C.; Schwiertz, D.; Scherer, M.; Bleher, S.; Süss, R.; Barz, M., Polysarcosine-Based Lipids: From Lipopolypeptoid Micelles to Stealth-Like Lipids in Langmuir Blodgett Monolayers. *Polymers* **2016,** 8, (12), 427.
23. Birke, A.; Ling, J.; Barz, M., Polysarcosine-containing copolymers: Synthesis, characterization, self-assembly, and applications. *Prog. Polym. Sci.* **2018,** 81, 163-208.
24. Fokina, A.; Klinker, K.; Braun, L.; Jeong, B. G.; Bae, W. K.; Barz, M.; Zentel, R., Multidentate Polysarcosine-Based Ligands for Water-Soluble Quantum Dots. *Macromolecules* **2016,** 49, (10), 3663-3671.
25. Hadjichristidis, N.; Iatrou, H.; Pitsikalis, M.; Sakellariou, G., Synthesis of Well-Defined Polypeptide-Based Materials via the Ring-Opening Polymerization of α-Amino Acid N-Carboxyanhydrides. *Chem. Rev.* **2009,** 109, (11), 5528-5578.
26. Zhang, D.; Lahasky, S. H.; Guo, L.; Lee, C.-U.; Lavan, M., Polypeptoid Materials: Current Status and Future Perspectives. *Macromolecules* **2012,** 45, (15), 5833-5841.
27. Birke, A.; Huesmann, D.; Kelsch, A.; Weilbächer, M.; Xie, J.; Bros, M.; Bopp, T.; Becker, C.; Landfester, K.; Barz, M., Polypeptoid-block-polypeptide Copolymers: Synthesis, Characterization, and Application of Amphiphilic Block Copolypept(o)ides in Drug Formulations and Miniemulsion Techniques. *Biomacromolecules* **2014,** 15, (2), 548-557.
28. Huesmann, D.; Sevenich, A.; Weber, B.; Barz, M., A head-to-head comparison of poly(sarcosine) and poly(ethylene glycol) in peptidic, amphiphilic block copolymers. *Polymer* **2015,** 67, 240-248.
29. Fetsch, C.; Gaitzsch, J.; Messager, L.; Battaglia, G.; Luxenhofer, R., Self-Assembly of Amphiphilic Block Copolypeptoids – Micelles, Worms and Polymersomes. *Sci. Rep.* **2016,** 6, 33491.
30. Weber, B.; Kappel, C.; Scherer, M.; Helm, M.; Bros, M.; Grabbe, S.; Barz, M., PeptoSomes for Vaccination: Combining Antigen and Adjuvant in Polypept(o)ide-Based Polymersomes. *Macromol. Biosci.* **2017,** 17, (10), 1700061.
31. Makino, A.; Hara, E.; Hara, I.; Ozeki, E.; Kimura, S., Size Control of Core–Shell-type Polymeric Micelle with a Nanometer Precision. *Langmuir* **2014,** 30, (2), 669-674.
32. Kim, C. J.; Ueda, M.; Imai, T.; Sugiyama, J.; Kimura, S., Tuning the Viscoelasticity of Peptide Vesicles by Adjusting Hydrophobic Helical Blocks Comprising Amphiphilic Polypeptides. *Langmuir* **2017,** 33, (22), 5423-5429.
33. Warren, N. J.; Mykhaylyk, O. O.; Mahmood, D.; Ryan, A. J.; Armes, S. P., RAFT aqueous dispersion polymerization yields poly(ethylene glycol)-based diblock copolymer nano-objects with predictable single phase morphologies. *J. Am. Chem. Soc.* **2014,** 136, (3), 1023-33.
34. Warren, N. J.; Armes, S. P., Polymerization-induced self-assembly of block copolymer nano-objects via RAFT aqueous dispersion polymerization. *J. Am. Chem. Soc.* **2014,** 136, (29), 10174-85.

35. Canning, S. L.; Smith, G. N.; Armes, S. P., A Critical Appraisal of RAFT-Mediated Polymerization-Induced Self-Assembly. *Macromolecules* **2016,** 49, (6), 1985-2001.
36. Derry, M. J.; Fielding, L. A.; Armes, S. P., Polymerization-induced self-assembly of block copolymer nanoparticles via RAFT non-aqueous dispersion polymerization. *Prog. Polym. Sci.* **2016,** 52, 1-18.
37. Wang, G.; Schmitt, M.; Wang, Z.; Lee, B.; Pan, X.; Fu, L.; Yan, J.; Li, S.; Xie, G.; Bockstaller, M. R.; Matyjaszewski, K., Polymerization-Induced Self-Assembly (PISA) Using ICAR ATRP at Low Catalyst Concentration. *Macromolecules* **2016,** 49, (22), 8605-8615.
38. Obeng, M.; Milani, A. H.; Musa, M. S.; Cui, Z.; Fielding, L. A.; Farrand, L.; Goulding, M.; Saunders, B. R., Self-assembly of poly(lauryl methacrylate)-b-poly(benzyl methacrylate) nano-objects synthesised by ATRP and their temperature-responsive dispersion properties. *Soft Matter* **2017,** 13, (11), 2228-2238.
39. Qiao, X. G.; Lansalot, M.; Bourgeat-Lami, E.; Charleux, B., Nitroxide-Mediated Polymerization-Induced Self-Assembly of Poly(poly(ethylene oxide) methyl ether methacrylate-co-styrene)-b-poly(n-butyl methacrylate-co-styrene) Amphiphilic Block Copolymers. *Macromolecules* **2013,** 46, (11), 4285-4295.
40. Qiao, X. G.; Dugas, P. Y.; Charleux, B.; Lansalot, M.; Bourgeat-Lami, E., Nitroxide-mediated polymerization-induced self-assembly of amphiphilic block copolymers with a pH/temperature dual sensitive stabilizer block. *Polym. Chem.* **2017,** 8, (27), 4014-4029.
41. Williams, M.; Penfold, N. J. W.; Lovett, J. R.; Warren, N. J.; Douglas, C. W. I.; Doroshenko, N.; Verstraete, P.; Smets, J.; Armes, S. P., Bespoke cationic nano-objects via RAFT aqueous dispersion polymerisation. *Polym. Chem.* **2016,** 7, (23), 3864-3873.
42. Blackman, L. D.; Doncom, K. E. B.; Gibson, M. I.; O'Reilly, R. K., Comparison of photo- and thermally initiated polymerization-induced self-assembly: a lack of end group fidelity drives the formation of higher order morphologies. *Polym. Chem.* **2017,** 8, (18), 2860-2871.
43. Deng, R.; Derry, M. J.; Mable, C. J.; Ning, Y.; Armes, S. P., Using Dynamic Covalent Chemistry To Drive Morphological Transitions: Controlled Release of Encapsulated Nanoparticles from Block Copolymer Vesicles. *J. Am. Chem. Soc.* **2017,** 139, (22), 7616-7623.
44. Khor, S. Y.; Truong, N. P.; Quinn, J. F.; Whittaker, M. R.; Davis, T. P., Polymerization-Induced Self-Assembly: The Effect of End Group and Initiator Concentration on Morphology of Nanoparticles Prepared via RAFT Aqueous Emulsion Polymerization. *ACS Macro Lett.* **2017,** 6, (9), 1013-1019.
45. Wright, D. B.; Touve, M. A.; Thompson, M. P.; Gianneschi, N. C., Aqueous-Phase Ring-Opening Metathesis Polymerization-Induced Self-Assembly. *ACS Macro Lett.* **2018,** 7, (4), 401-405.
46. Foster, J. C.; Varlas, S.; Blackman, L. D.; Arkinstall, L. A.; O'Reilly, R. K., Ring-Opening Metathesis Polymerization in Aqueous Media Using a Macroinitiator Approach. *Angew. Chem. Int. Ed.* **2018,** 57, (33), 10672-10676.
47. Wright, D. B.; Touve, M. A.; Adamiak, L.; Gianneschi, N. C., ROMPISA: Ring-Opening Metathesis Polymerization-Induced Self-Assembly. *ACS Macro Lett.* **2017,** 6, (9), 925-929.
48. Tan, J.; Sun, H.; Yu, M.; Sumerlin, B. S.; Zhang, L., Photo-PISA: Shedding Light on Polymerization-Induced Self-Assembly. *ACS Macro Lett.* **2015,** 4, (11), 1249-1253.
49. Yeow, J.; Xu, J.; Boyer, C., Polymerization-Induced Self-Assembly Using Visible Light Mediated Photoinduced Electron Transfer–Reversible Addition–Fragmentation Chain Transfer Polymerization. *ACS Macro Lett.* **2015,** 4, (9), 984-990.

50. Tan, J.; Bai, Y.; Zhang, X.; Zhang, L., Room temperature synthesis of poly(poly(ethylene glycol) methyl ether methacrylate)-based diblock copolymer nano-objects via Photoinitiated Polymerization-Induced Self-Assembly (Photo-PISA). *Polym. Chem.* **2016,** 7, (13), 2372-2380.
51. Ng, G.; Yeow, J.; Xu, J.; Boyer, C., Application of oxygen tolerant PET-RAFT to polymerization-induced self-assembly. *Polym. Chem.* **2017,** 8, (18), 2841-2851.
52. Tan, J.; Liu, D.; Bai, Y.; Huang, C.; Li, X.; He, J.; Xu, Q.; Zhang, X.; Zhang, L., An insight into aqueous photoinitiated polymerization-induced self-assembly (photo-PISA) for the preparation of diblock copolymer nano-objects. *Polym. Chem.* **2017,** 8, (8), 1315-1327.
53. Yeow, J.; Boyer, C., Photoinitiated Polymerization-Induced Self-Assembly (Photo-PISA): New Insights and Opportunities. *Adv. Sci.* **2017,** 4, (7), 1700137.
54. Burridge, K. M.; Wright, T. A.; Page, R. C.; Konkolewicz, D., Photochemistry for Well-Defined Polymers in Aqueous Media: From Fundamentals to Polymer Nanoparticles to Bioconjugates. *Macromol. Rapid Commun.* **2018,** 39, (12), 1800093.
55. Tan, J.; Zhang, X.; Liu, D.; Bai, Y.; Huang, C.; Li, X.; Zhang, L., Facile Preparation of CO2-Responsive Polymer Nano-Objects via Aqueous Photoinitiated Polymerization-Induced Self-Assembly (Photo-PISA). *Macromol. Rapid Commun.* **2016,** 38, (13), 1600508.
56. Tan, J.; Liu, D.; Bai, Y.; Huang, C.; Li, X.; He, J.; Xu, Q.; Zhang, L., Enzyme-Assisted Photoinitiated Polymerization-Induced Self-Assembly: An Oxygen-Tolerant Method for Preparing Block Copolymer Nano-Objects in Open Vessels and Multiwell Plates. *Macromolecules* **2017,** 50, (15), 5798-5806.
57. Blackman, L. D.; Varlas, S.; Arno, M. C.; Fayter, A.; Gibson, M. I.; O'Reilly, R. K., Permeable Protein-Loaded Polymersome Cascade Nanoreactors by Polymerization-Induced Self-Assembly. *ACS Macro Lett.* **2017,** 6, (11), 1263-1267.
58. Blackman, L. D.; Varlas, S.; Arno, M. C.; Houston, Z. H.; Fletcher, N. L.; Thurecht, K. J.; Hasan, M.; Gibson, M. I.; O'Reilly, R. K., Confinement of Therapeutic Enzymes in Selectively Permeable Polymer Vesicles by Polymerization-Induced Self-Assembly (PISA) Reduces Antibody Binding and Proteolytic Susceptibility. *ACS Cent. Sci.* **2018,** 4, (6), 718-723.
59. Varlas, S.; Blackman, L. D.; Findlay, H. E.; Reading, E.; Booth, P. J.; Gibson, M. I.; O'Reilly, R. K., Photoinitiated Polymerization-Induced Self-Assembly in the Presence of Surfactants Enables Membrane Protein Incorporation into Vesicles. *Macromolecules* **2018,** 51, (6), 6190-6201.
60. Weber, B.; Birke, A.; Fischer, K.; Schmidt, M.; Barz, M., Solution Properties of Polysarcosine: From Absolute and Relative Molar Mass Determinations to Complement Activation. *Macromolecules* **2018,** 51, (7), 2653-2661.
61. Johnson, R. N.; Burke, R. S.; Convertine, A. J.; Hoffman, A. S.; Stayton, P. S.; Pun, S. H., Synthesis of Statistical Copolymers Containing Multiple Functional Peptides for Nucleic Acid Delivery. *Biomacromolecules* **2010,** 11, (11), 3007-3013.
62. Bilalis, P.; Tziveleka, L.-A.; Varlas, S.; Iatrou, H., pH-Sensitive nanogates based on poly(l-histidine) for controlled drug release from mesoporous silica nanoparticles. *Polym. Chem.* **2016,** 7, (7), 1475-1485.
63. Tan, J.; He, J.; Li, X.; Xu, Q.; Huang, C.; Liu, D.; Zhang, L., Rapid synthesis of well-defined all-acrylic diblock copolymer nano-objects via alcoholic photoinitiated polymerization-induced self-assembly (photo-PISA). *Polym. Chem.* **2017,** 8, (44), 6853-6864.
64. Robertson, J. D.; Yealland, G.; Avila-Olias, M.; Chierico, L.; Bandmann, O.; Renshaw, S. A.; Battaglia, G., pH-Sensitive Tubular Polymersomes: Formation and Applications in Cellular Delivery. *ACS Nano* **2014,** 8, (5), 4650-4661.

TABLE OF CONTENTS GRAPHIC (TOC)

"Poly(sarcosine)-Based Nano-Objects with Multi-Protease Resistance by Aqueous Photoinitiated Polymerization-Induced Self-Assembly (Photo-PISA)"

Spyridon Varlas,[a] Panagiotis G. Georgiou,[a,b] Panayiotis Bilalis,[c] Joseph R. Jones,[a] Nikos Hadjichristidis,[c] and Rachel K. O'Reilly[a]**

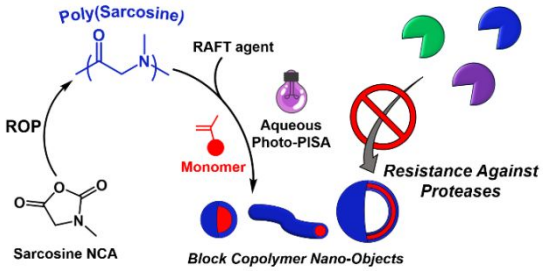

Poly(sarcosine)-based diblock copolymer nano-objects with various morphologies were prepared by combining *N*-carboxyanhydride ring-opening polymerization (ROP) and RAFT-mediated photoinitiated polymerization-induced self-assembly (photo-PISA) of a commercially available monomer (2-hydroxypropyl methacrylate), using a poly(sarcosine) macromolecular chain transfer agent. Based on a constructed phase diagram, vesicles were chosen and the resistance of both empty and horseradish peroxidase-loaded ones against degradation by a series of proteolytic enzymes was evaluated.